Effect of Nb and V Doped Elements on the Mechanical and Tribological Properties of CrYN Coatings

Gokhan Gulten[1], Banu Yaylali[1], Ihsan Efeoglu[1*], Yasar Totik[1], Peter Kelly[2] and Justyna Kulczyk-Malecka[2]

[1]Faculty of Engineering, Department of Mechanical Engineering, Atatürk University, 25240 Erzurum, Türkiye

[2] Surface Engineering Group, Manchester Metropolitan University, Manchester M1 5GD, UK

*Corresponding author.

E-mail address: iefeoğlu@atauni.edu.tr (Ihsan Efeoglu)

Abstract

One of the most promising approaches to enhancing the tribological properties of engineering coatings is to add transition elements to the structure. In this study, Nb-doped CrYN and V-doped CrYN thin films were deposited by pulsed DC reactive sputtering in a closed-field unbalanced magnetron sputtering (CFUBMS) system. The deposition parameters examined were target current (1, 1.5 and 2 A), deposition pressure (0.15, 0.25 and 0.35 Pa), pulse frequency (100, 200 and 350 kHz) and duty cycle (85%, 70% and 50%). A Taguchi L9 orthogonal design was used to define the deposition process parameters for each doped film. The Nb and V-doped CrYN thin films were characterized in terms of their microstructure, thickness, composition, hardness and tribological properties by X-ray diffraction (XRD), scanning electron microscopy (SEM), Energy dispersive spectroscopy (EDS), X-ray photoelectron spectroscopy (XPS), nanohardness and pin-on-disc testing, respectively. The bond strength between the substrate and the films (adhesion) was analyzed by scratch testing. For the Nb-doped thin films, a maximum hardness value of 21.4 GPa and the lowest friction coefficient of 0.36 were obtained. On the other hand, in the V-doped thin films, the maximum hardness value was 16.1 GPa, while the lowest friction coefficient obtained was 0.11. In addition, Nb-doped and V-doped CrYN thin films exhibited extraordinary adhesion properties. The effect of the selected deposition parameters (target current, pulse frequency, and duty cycle) in relation to the film thickness, hardness, and coefficient of friction properties of the Nb and V-doped CrYN thin films were investigated using the Taguchi approach and optimum operating conditions were identified and confirmed.

Keywords: Transition metal nitride, Nb/V doped elements, reactive magnetron sputtering

1. Introduction

The degradation of material surfaces operating within hostile environments, resulting in damage, is a key challenge typically encountered in industrial applications. Thin films with functional qualities are used to improve the properties of operational surfaces. For example, functional thin films produced from transition metal nitrides (such as Cr, Ti, Nb, Zr, V, Ta, nitrides and others) are applied to surfaces using a variety of modern thin film processes, exhibiting remarkable mechanical and tribological properties, even when exposed to extreme environments [1–5]. The most widely used transition metal nitride thin film is titanium nitride (TiN). TiN thin films, due to their outstanding properties and performance characteristics, have emerged as a desirable and multifunctional material in a variety of industries. However, one of the primary disadvantages is their susceptibility to oxidation at elevated temperatures. TiN thin films begin to oxidize at temperatures around 500°C, leading to the formation of titanium oxide (TiO_2) and a reduction in their wear resistance and mechanical properties. CrN thin films, exhibit better oxidation resistance (up to 700°C) compared to TiN thin films [6–9]. However, the performance of CrN thin films in more harsh environments is insufficient and many research studies have been done to enhance the structural, mechanical, tribological, and oxidation efficiency of these thin films by doping with different elements such as aluminum, silicon, molybdenum, niobium, and vanadium [10–13]. Additionally, it has been found that the existence of substitutional atoms in the structure, such as Y atoms, improves thermal and oxidation resistance over a certain temperature range, because they significantly slow down the diffusion-related processes [14].

Hones et al. deposited Nb-doped CrN thin films using the reactive magnetron sputtering technique and suggested that Nb doping had an improving effect on the hardness and elastic modulus of the thin films [15]. Chang et al. reported that Nb-doped CrN possesses better corrosion resistance due to its higher polarization resistance and lower capacitance [16]. Liu et al. found that an effective enhancement was achieved in terms of friction coefficient and wear rate, through the addition of Nb to the thin film structure by increasing the film hardness and plastic deformation resistance [17]. In comparison to Nb-doped CrN thin films, fewer V-doped CrN thin films have been studied. Nevertheless, several researchers have reported that V-doped CrN films exhibit a low coefficient of friction and wear rate, especially in aggressive environments such as high temperatures [18,19].

In this study, thin films of both Nb-doped CrYN and V-doped CrYN were deposited using reactive closed-field unbalanced magnetron sputtering (CFUBMS) with different deposition

parameters. A Taguchi L9 orthogonal design was used to define the deposition conditions for each doped film. The deposition parameters (target current, pulse frequency and duty cycle, at three levels each) were investigated in terms of their impact on hardness, adhesion, and coefficient of friction properties of Nb-doped and V-doped thin films.

2. Materials and Methods

Nb-doped CrYN and V-doped CrYN thin films were deposited on AISI 316 L, glass, and Si (111) substrates via CFUBMS in a Teer Coating Ltd. UDP550 coating rig under different deposition parameters, based on a Taguchi L9 orthogonal design. Microstructural investigations were performed on the coated silicon and glass substrates. Table 1 lists the deposition parameters, and Fig. 1 shows the magnetron configuration of the targets in order to deposit Nb-doped and V-doped thin films and the architectural structure of the films. Prior to deposition, the AISI 316L substrates were ultrasonically cleaned and polished with 400, 600, 800, and 1200 abrasive papers to achieve surface roughness values of 0.02 µm (Ra).

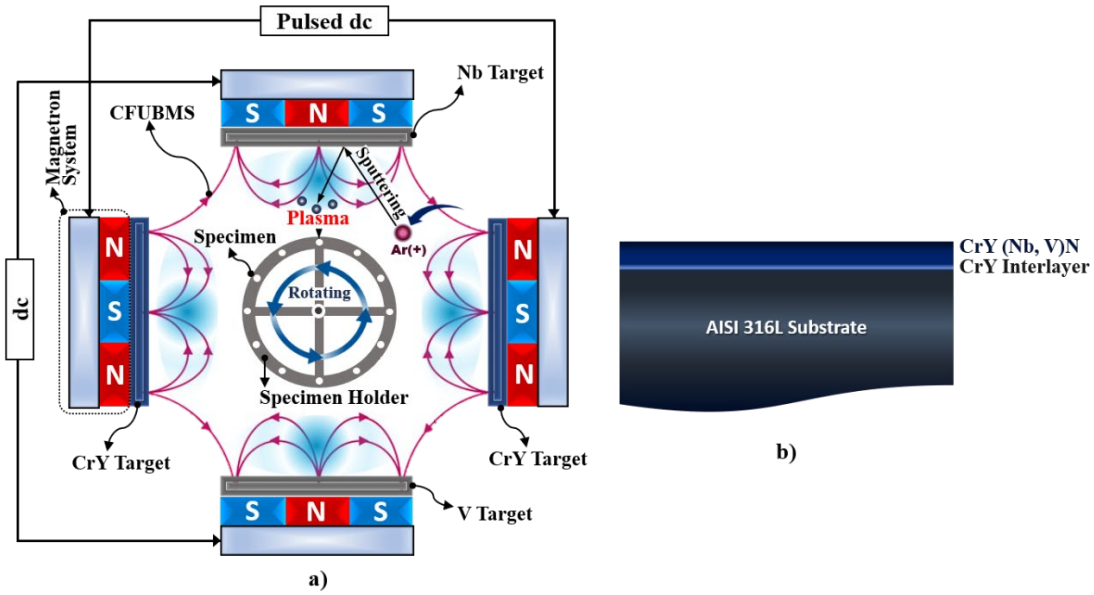

Fig. 1. a) Magnetron sputtering system and **b)** The arhitecture structure of Nb and V-doped CrYN thin films

Table 1. Deposition parameters levels and variables of Nb and V-doped CrYN thin films [20]

The variable Parameters	**Level 1**	**Level 2**	**Level 3**
CrY Target Current (A)	1	1.5	2
Deposition Pressure (Pa)	0.15	0.25	0.35
Pulse Frequency (kHz)	100	200	350
Duty Cycle (%)	50	70	85
The Constant Parameters			
CrY Interlayer		CrY: 2A (10 min)	
CrY (Nb, V)N		Nb: 2A, V:2A (90 min)	
N_2 Flow Rate (sccm)		6	
Substrate Bias (-V)		50	

Table 2. Experimental runs for Nb and V-doped CrYN thin films [20]

	Pulse Frequency (kHz)	Duty Cycle (%)	Deposition Pressure (Pa)	CrY Target Current (A)
R1	100	50	0.15	1
R2	100	70	0.25	1.5
R3	100	85	0.35	2
R4	200	50	0.25	2
R5	200	70	0.35	1
R6	200	85	0.15	1.5
R7	350	50	0.35	1.5
R8	350	70	0.25	2
R9	350	85	0.15	1

In the process, two CrY (%99.95 pure) and one Nb (%99.95 pure) or V (%99.95 pure) targets were used to deposit Nb-doped and V-doped thin films, depending on the film type. The CrY target used consists of 97% at. Cr and 3% at. Y. The Advanced Energy Pinnacle Plus pulsed-DC power supply was connected to the CrY targets, whereas an Advanced Energy Pinnacle DC power supply was connected to the Nb or V targets. The gas ratios (Ar and N_2) in the chamber during film deposition were controlled by mass flow controllers (MKS system). The chamber pressure is controlled throughout the deposition process. While the N_2 flow was kept at 6 sccm for all runs, the Ar flow was changed between 10-20 sccm for the variable deposition pressures given in Table 2. The substrates are fixed to a system that rotates (one-degree rotation) around its axis in front of the targets. The distance between the substrates and the targets was set to 70 mm at the closest point. Before the deposition process, ion cleaning was carried out for 30 minutes by applying 800 V of negative bias voltage (DC) to the substrates in an argon atmosphere. This process is carried out in order to remove any existing contaminants and improve the adhesion between the substrate and the film. After ion cleaning, the CrY interlayer was deposited for 10 minutes in order to further enhance the adhesion between the substrate and the film by effectively grading the film from a metallic layer to a ceramic layer without an abrupt transition. During the deposition of the CrY interlayer, the current applied to the CrY targets was fixed at 2A for all films. The Nb-doped CrYN or V-doped CrYN layers were then deposited for 90 min. During the deposition of the Nb and V-doped CrYN layer, the Taguchi L9 orthogonal design parameters in Table 2 were used for all runs. The response of specific properties, e.g. film hardness, to these conditions is expressed by calculating the average response for each level of array parameter, referred to as the 'level average'.

The deposited Nb-doped and V-doped thin films were microstructurally analyzed using a Zeiss Sigma 300 Scanning Electron Microscope (SEM/EDS). Elemental composition of the thin films was conducted with Specs-Flex X-ray photoelectron spectroscopy (XPS). The crystal structures of the deposited thin films were examined by XRD using a Rigaku DMax-2200 type (Cu-Kα:

1.5405 radiation source and 30-100° scan range). The nanohardness values of the deposited thin films were examined using a Anton Paar Step 500 nanohardness tester (using a Berkovich indenter, 3mN load at 25 different points). The critical load values of the deposited thin films were determined from 3 different points using a CSM Instruments scratch tester. (100 N/min progressive loading rate, 200 tip radius with a Rockwell-C diamond indenter). A CSM tribotester (1 N load, 10 cm/s velocity, 6.25 mm diameter Al_2O_3 counterpart) was used to determine the tribological properties of the deposited thin films in ambient air.

3. Results and discussions

The film thicknesses and surface morphology were determined by investigating the cross-sectional surfaces obtained by radial fractures of the Nb and V-doped thin films that were deposited on Si (111) substrates. Typical cross-sectional SEM micrographs of Nb and V-doped CrYN thin films are given in Figs. 2a and 2b. Film thickness values of these films, measured from the fracture sections are given in Figs. 3a and 3c. SEM examination of cross-sections of the thin films generally exhibited the existence of a dense and uniform structure. The formation of a dense structure is due to the pulsed-DC power supply, which provides a more stable process by eliminating arc and microarc formation to a large extent and produces a more energetic plasma than a continuous DC plasma [21]. According to the Figs. 3a and 3c, the highest film thickness was obtained in the experiment (R3) where the lowest pulse frequency, highest duty cycle, lowest pressure and highest target current were applied. Lowering the pulse frequency causes an increase in peak current. This increase in peak current increases the ionization rate of the sputtered atoms. A high ionization rate means more atoms or molecules are ionized during the sputtering process and the film thickness increases[22]. Also, increasing the current enhances the ion flux impacting the target surface, leading to higher sputtering rates [23]. Moreover, the duty cycle is the time the power is on relative to the total cycle time in pulsed sputtering processes. A higher duty cycle indicates a greater bombardment of the target material with ions, resulting in more atoms being sputtered. This increases the number of atoms reaching the substrate, resulting in a higher deposition rate [24].

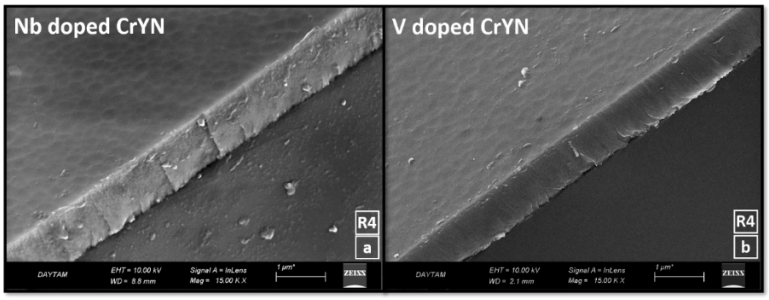

Fig 2. Typical cross-sectional SEM micrographs of **a)** Nb-doped (R4) and **b)** V-doped CrYN (R4) thin film

Fig. 3b and 3d shows the level averages (larger is better) for the film thickness. Level averages (larger is better) are used to calculate the response. The S/N response showed in Figs. 3b and 3d was derived using the Taguchi Design of Experiments (DOE) method in Minitab software (version 21.3.1). We employed Analysis of Variance (ANOVA) to evaluate the percentage contribution of various process parameters on the film thickness. As per Fig. 3b and 3d, the contribution levels of pulse frequency, duty cycle, deposition pressure, and CrY target current, as determined by the ANOVA analysis, are 40.10%, 21.59%, 3.97%, and 34.34% respectively for Nb-doped CrYN films. For V-doped CrYN thin films, the contribution levels of pulse frequency, duty cycle, deposition pressure, and CrY target current are 68.67%, 7.09%, 9.38%, and 14.85%, respectively.

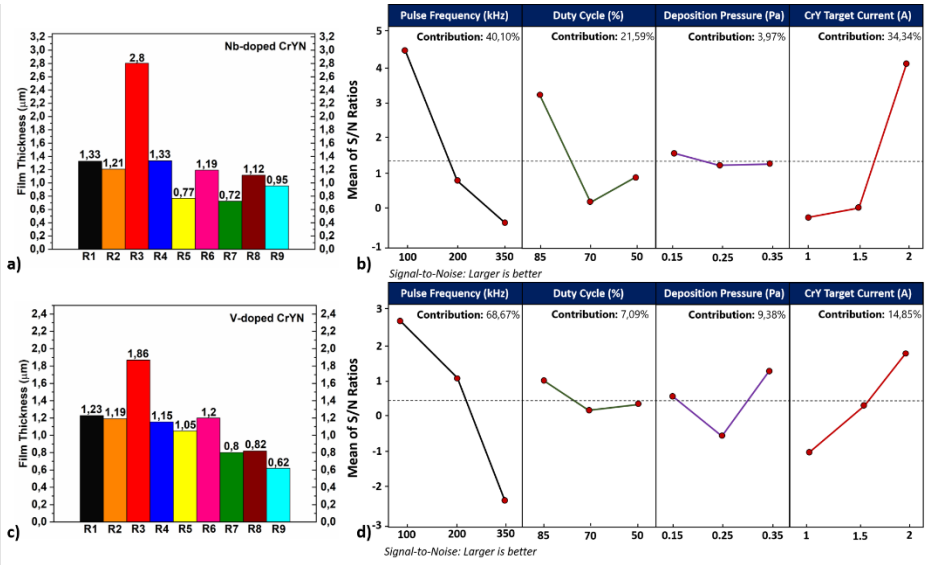

Fig 3. a) Film thickness of Nb-doped thin films, **b)** Average S/N Ratios for Nb-doped thin films in thickness, **c)** film thickness of V-doped thin films and, **d)** Average S/N Ratios for V-doped thin films in thickness

Table 3. Elemental composition of Nb doped CrYN thin films

		R1	R2	R3	R4	R5	R6	R7	R8	R9
at. %	Cr	44.09	34.64	73.33	56.21	41.54	57.97	39.9	55.29	31.25
	Y	0.99	1.21	1.56	0.93	0.88	1.03	0.75	0.76	0.61
	Nb	16.54	10.63	4.73	13.19	15.22	11.67	16.06	15.04	17.82
	N	38.39	34.64	20.39	29.67	42.37	29.33	43.28	28.91	50.32

Table 4. Elemental composition of V doped CrYN thin films

		R1	R2	R3	R4	R5	R6	R7	R8	R9
at. %	Cr	45.07	43.04	60.16	47.06	46.29	48.76	33.71	49.67	32.18
	Y	0.87	0.93	1.28	0.71	0.92	0.87	0.60	0.63	0.56
	V	18.78	16.94	12.68	19.59	17.03	18.19	17.29	19.98	18.01
	N	35.29	39.09	25.88	32.64	35.76	32.18	48.40	29.72	49.24

The EDS results of the Nb doped and V doped CrYN thin films are given in Table 3 and Table 4, respectively. In the Taguchi experimental setup, the experiments (R3, R4, and R8) with the

highest CrY target current applied showed the highest amounts of Cr and Y. The primary reason for the Y ratio being between 0.5-1.6 is that the used CrY targets contain 97% Cr and 3% Y. The increase in nitrogen content can be attributed to a decrease in pressure. Because, the working pressure and N_2/Ar are inversely proportional. Since the N_2 flow did not change in these experiments, the Argon ratio was varied in certain ratios to keep the working pressure constant with the MKS system.

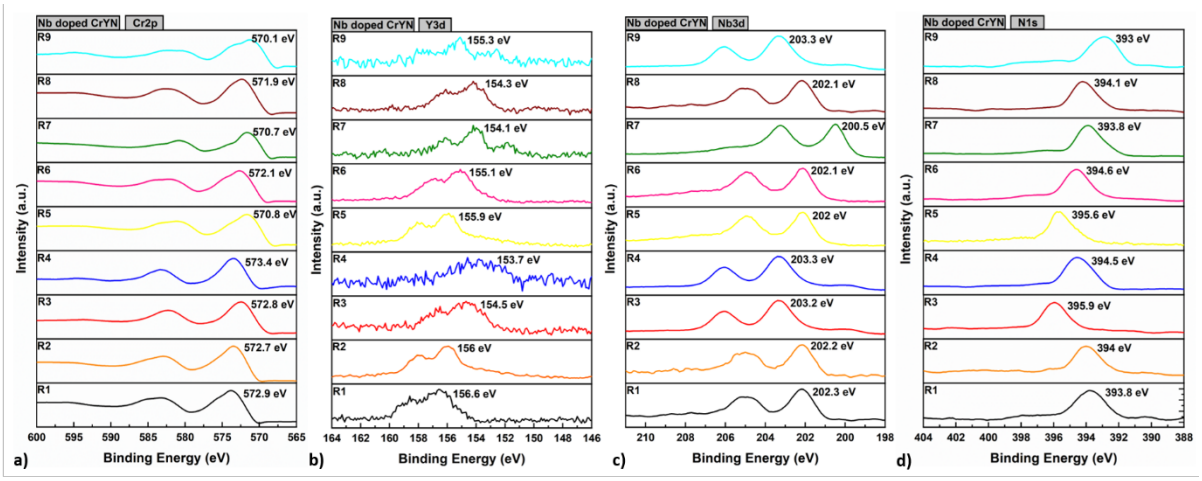

Fig. 4. a) Cr2p spectra of Nb-doped thin films, **b)** Y3d spectra of Nb-doped thin films, **c)** Nb3d spectra of Nb-doped thin films and, **d)** N1s spectra of Nb-doped thin films

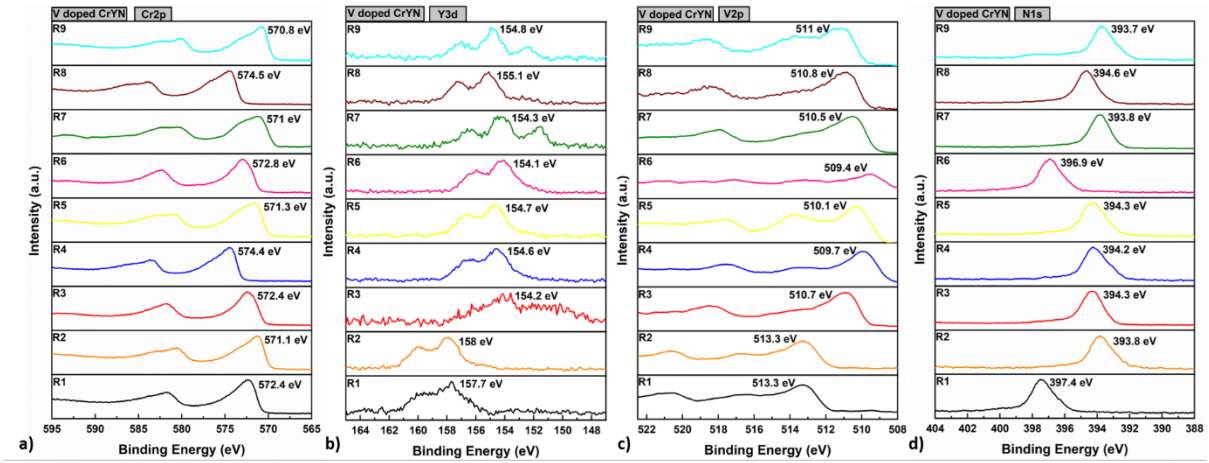

Fig. 5. a) Cr2p spectra of V-doped thin films, **b)** Y3d spectra of V-doped thin films, **c)** Nb3d spectra of V-doped thin films and, **d)** N1s spectra of V-doped thin films

X-ray photoelectron spectroscopy is a powerful analytical technique used to determine the chemical state and binding energies of elements on material surfaces. XPS spectra display the binding energies of photoelectrons, and a shift in these energies can indicate changes in the material's chemical and physical properties. Figs. 5 and 6 show the XPS core-level spectra of Nb and V-doped CrYN thin films. Also, In Fig. 6, the partial scanning XPS results (Gaussian deconvoluted) for the R5 sample have been analyzed. According to Fig. 4, the binding energies of $Cr2p_{3/2}$, $Y3d_{5/2}$, $Nb3d_{5/2}$, and N1s were identified as 570 ± 2, 150 ± 6, 200 ± 3, and 393 ± 3

eV, respectively. In Fig. 5, the binding energies of $Cr2p_{3/2}$, $Y3d_{5/2}$, $V2p_{3/2}$, and N1s were identified as 570.5 ± 4, Y3d, 509 ± 4, and 393 ± 4 eV, respectively. A noticeable shift in binding energies was observed in any of the peaks analyzed (Cr, Y, Nb, V and N). It is well-established in the literature that the binding energies of Cr 2p and N 1s decrease with an increase in nitrogen content[25–27]. The observed decrease in binding energy suggests that as the nitrogen content increases, the ability of electrons surrounding ionized chromium atoms to protect nuclear holes becomes less efficient. Additionally, Bertóli et al.[28] have demonstrated that the N 1s peak typically shows a broadening in the range of 1.6 to 1.9 eV, and any significant broadening is usually indicative of the presence of a new chemical state. These bonds in our case might correspond to CrN, Cr_2N, NbN, or VN (see Fig. 6).

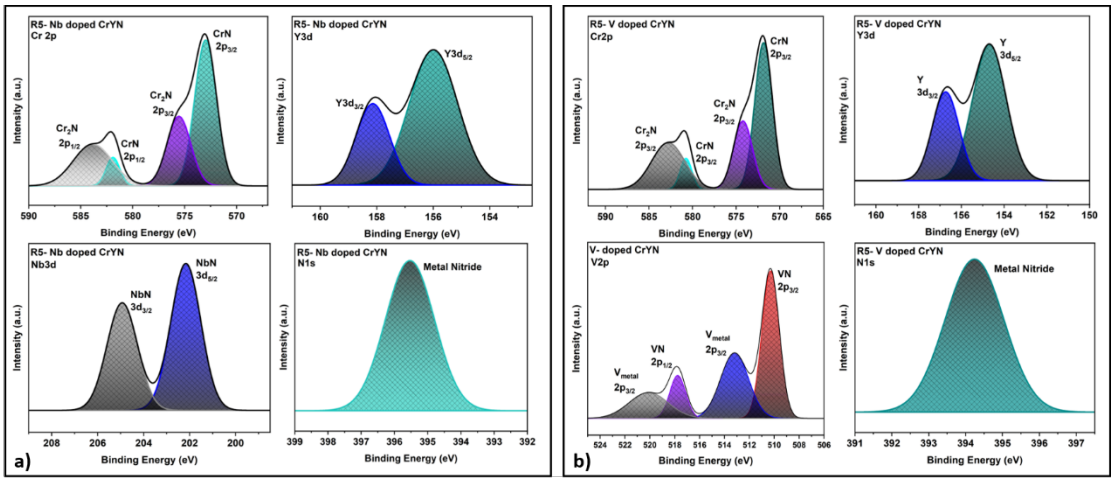

Fig. 6. X-ray photoelectron spectrum in the region of the **a)** Cr2p, Y3d, Nb3d and N1s for Nb doped CrYN **b)** Cr2p, Y3d, V2p and N1s for V doped CrYN

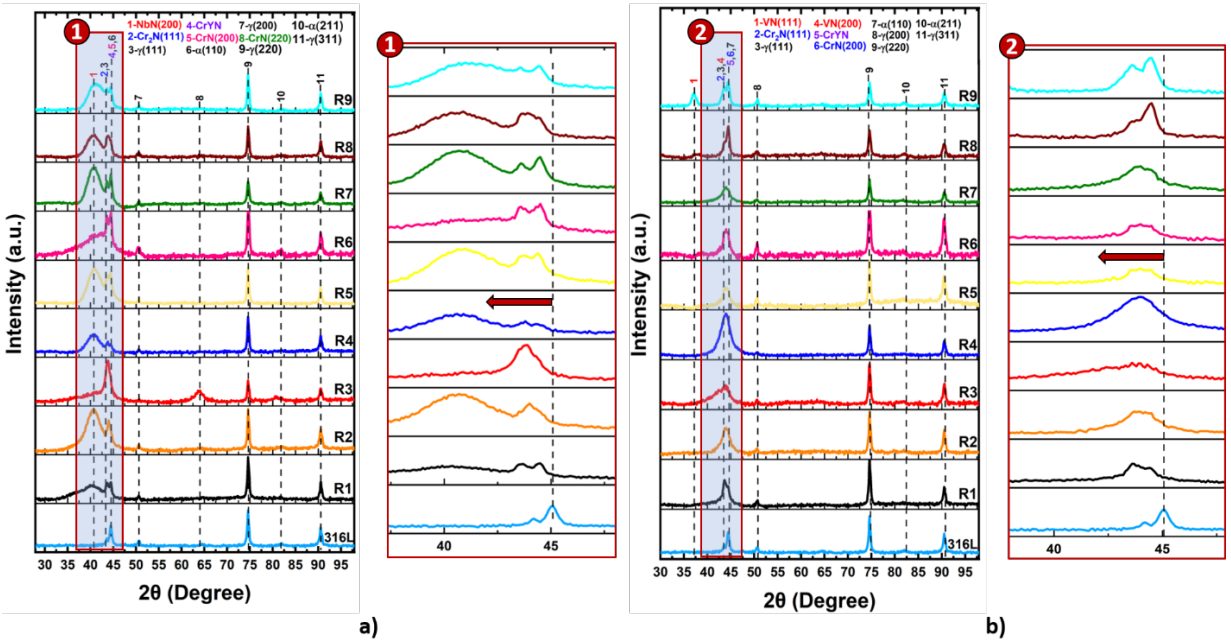

Fig. 7. XRD graphs of; **a)** Nb-doped CrYN thin films and, **b)** V-doped CrYN thin films

The XRD patterns of the Nb and V-doped CrYN thin films on 316 L substrates, as produced via various deposition parameters, are shown in Table 1 and Table 2. The crystalline structures of all deposited films were typically cubic. When Fig. 7a is examined, it is seen that the CrN peaks slightly shift to the left and broadening accordance with the 316L Substrate XRD peak. A possible reason for this is that the XRD peaks tend to shift towards a lower angle, due to compressive stress occurring in the coatings during sputtering. When the crystal lattice expands due to substitution, the spacing (d) between the planes will increase. According to Bragg's law, if (d) increases and (λ) remains constant, then θ (the angle of reflection) will decrease to satisfy the equation. This means that the angle at which maximum X-ray reflection occurs will shift to lower values. Thus, the X-ray diffraction pattern will shift, reflecting the changes in the lattice spacing. [29]. The peak shift can also be associated to the enhanced substitution of Y into the CrN, NbN and VN lattice structures. The higher ionic radius of Y (90 pm) relative to Cr (64 pm), Nb (64 pm), and V (59 pm) leads to a broadening in the lattice. Examining Fig. 7a and 7b shows that the intensity of the CrN and Cr_2N crystal phases increases with increasing pulse frequency, duty time, and current applied to the CrY targets.

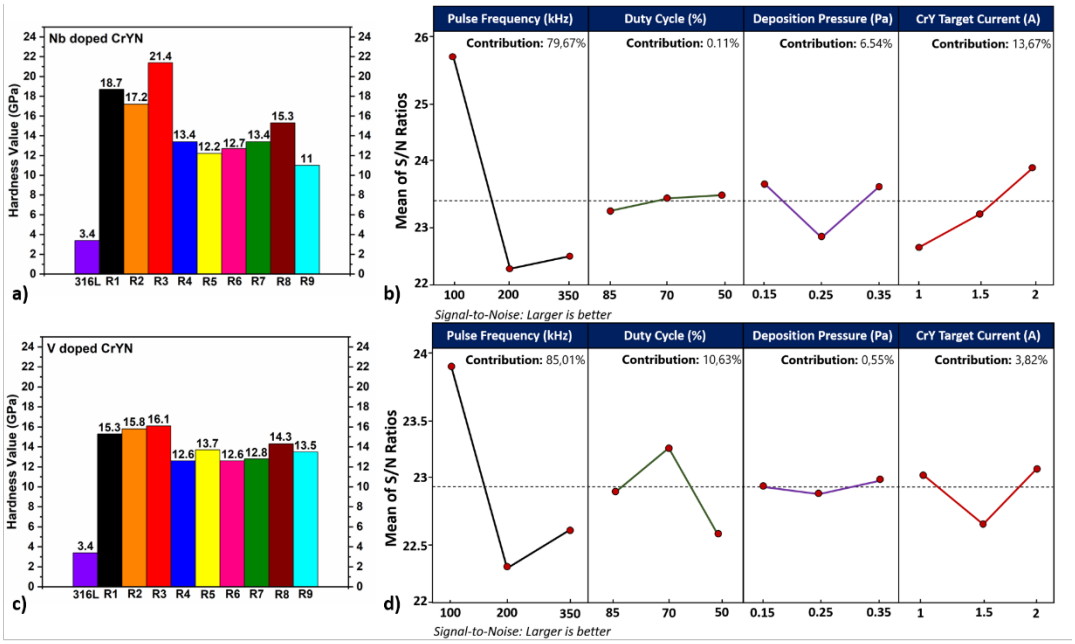

Fig. 8. a) Hardness value of Nb-doped thin films, **b)** Average S/N Ratios for Nb-doped thin films in hardness, **c)** Hardness value of V-doped thin films and **d)** Average S/N Ratios for V-doped thin films in hardness

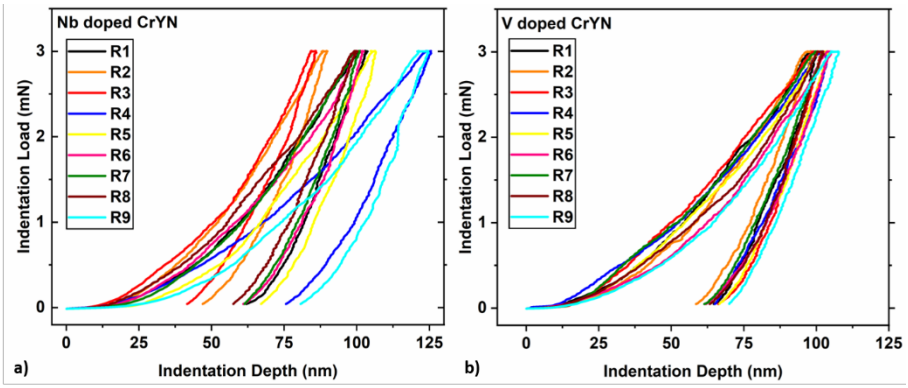

Fig. 9. Nanoindentation curves **a)** Nb-doped CrYN thin films **b)** V-doped CrYN thin films

Nano-hardness, also known as nanoindentation, is a technique for measuring the mechanical properties of materials at the nanoscale, specifically hardness and elastic modulus. It involves applying a controlled force to the surface of a material with a sharp indenter (Berkovich indenter) and measuring the indentation depth. This sensitive technique can be used to investigate the mechanical properties of thin films. The maximum indentation depth for Nb and V-doped thin films had to be less than 100 nm. This depth penetration is sufficiently small to avoid the size indentation effect, which typically needs to be less than 10% of the film thickness to avoid the substrate influencing the hardness value. The hardness values obtained by the nanoindentation technique are shown in Figs. 8a and 8c. Figs. 9a and 9b also show nanoindentation curves. The maximum hardness value obtained for Nb-doped thin films was 21.4 GPa for R3. Although the hardness values obtained in V-doped films are relatively similar (see Fig 9b), the highest hardness values obtained was 16.1 GPa for R3. The S/N response showed in Figs. 8b and 8d was derived using the Taguchi DOE method in Minitab software, which employs Analysis of Variance (ANOVA) to evaluate the percentage contribution of various process parameters on the film hardness. As per Figs. 8b and 8d, the contribution levels of pulse frequency, duty cycle, deposition pressure, and CrY target current, as determined by the ANOVA analysis, are 79.67%, 0.11%, 6.54%, and 13.67% respectively for Nb-doped CrYN films. For V-doped CrYN thin films, the contribution levels of pulse frequency, duty cycle, deposition pressure, and CrY target current are 85.01%, 10,63%, 0,55%, and 3,82%, respectively. Figs. 8b and 8d show that for both doped films, the pulse frequency with the highest delta is the most effective parameter for film hardness. It is generally known that the hardness and elastic modulus of coatings can be associated to differences in microstructure, residual stress, and chemical composition.

Scratch testing was applied to determine the adhesion properties of Nb-doped and V-doped CrYN thin films. The adhesion properties of Nb-doped and V-doped CrYN thin films were found to be outstanding. The coating remained on the surface of the substrate in all tests up to

an applied load of 150N. Since similar properties were obtained for all runs, the scratch results of the R6 film, which typically have the closest film thickness and film hardness values for Nb and V-doped films, are given in Figs. 10 and 11 as examples. In Fig. 10, the results of the scratch test performed between 0 and 150N are given together with the optical microscope images. In adhesion testing, "Lc" usually refers to "a critical load" at which specific types of coating failure occur and is used as a measure of the coating's adhesion strength. The critical load values are classified as Lc1, Lc2, and Lc3. The critical load value at which the first crack or delamination occurs is defined by Lc1. Lc2 is the critical load value at which the coating's adhesion considerably fails and/or larger cracks occur. Finally, Lc3 defines the critical load value at which the film is completely delaminated and/or completely separated from the surface. In all the Nb and V-doped thin films, Lc2 and Lc3 were not observed, only a Lc1 value was determined. According to Fig. 10, no edge failures were detected in the range of 0-10N in Nb-doped thin films. After the value of 20N, bucking failures started to appear and continued to increase until the value of 150N. This type of damage is usually caused by compressive stresses in front of the moving indenter tip and adversely affects the mechanical properties of the film [30]. In Nb-doped thin films, relatively small size cracks started to form in the film structure at 20N, the crack size increased as the applied load value increased and the film continued to exist on the surface as smaller regions. The Lc1 value was determined at 40N. Adhesion failures continued to grow relatively with the increase of cracks from 40N. Since the film is harder than the substrate (see Fig. 8a), as the load value increased, the film was embedded in the substrate and continued to adhere to the surface. Similar characteristics are found for scratch test results of the V-doped thin films (Fig. 11). However, no edge failures were observed up to about 40N. In addition, buckling failures started after 40N. The cracks formed in the film are relatively smaller than those observed for the Nb-doped thin films. Adhesion failures observed at 150N were relatively fewer than for the Nb-doped thin films.

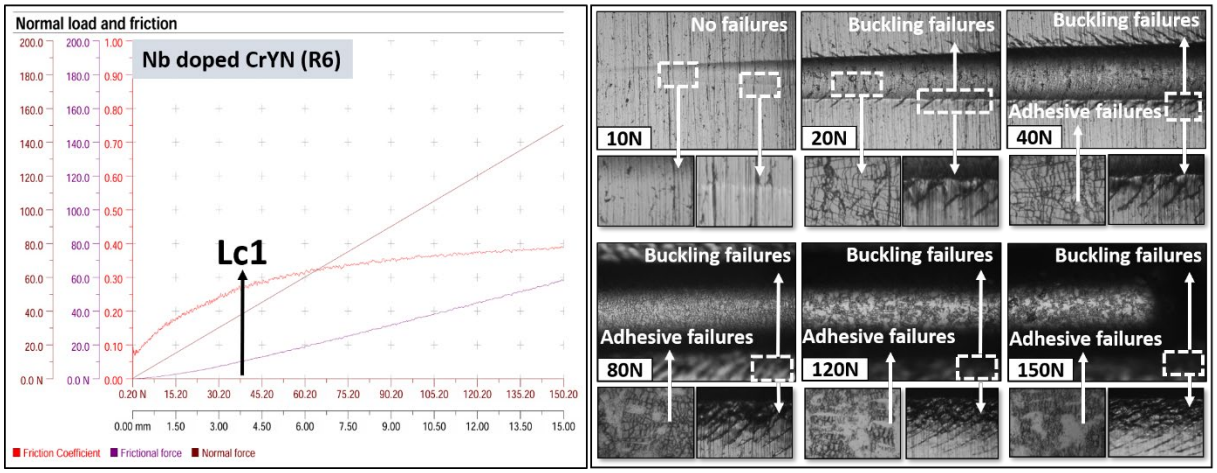

Fig. 10. Scratch test results for Nb doped CrYN (R6) thin films

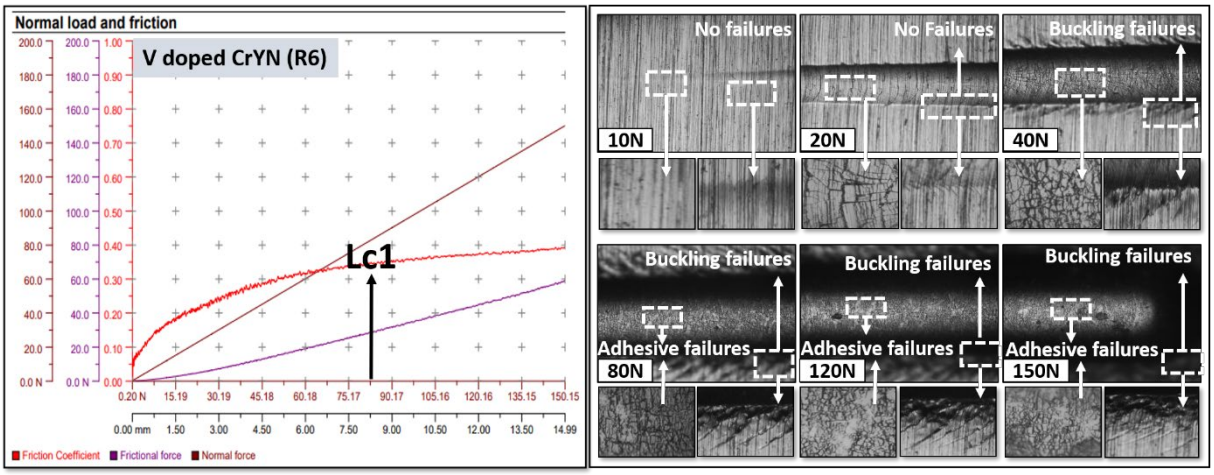

Fig. 11. Scratch test results for Nb doped CrYN (R6) thin films

A pin-on-disc wear test was carried out to investigate the tribological properties of the Nb and V-doped CrYN thin films under ambient atmospheric conditions. The coefficient of friction values of Nb and V-doped CrYN thin films for all runs are given in Figs. 12a and 12c, respectively. The lowest coefficient of friction (CoF) was found to be 0.36 and the maximum CoF was 0.77 in the Nb-doped thin films. The CoF of V-doped thin films, in contrast, ranged from 0.1 to 0.26, which is quite low in comparison. Considering the CoF behaviors of Nb-doped thin films in atmospheric conditions, it is clearly seen that they show a non-linear behavior. This can be explained by the continuous formation and rupture of the adhesive bond between the film and its counterpart. In addition, when the optical microscope images of the pin and wearing surfaces obtained after the friction test given in Fig. 13 are examined, it is seen that a large amount of wear debris has accumulated at the contact point. These wear particles formed at the contact point caused three-body abrasive wear, affect the linear behavior of the friction coefficient, and caused the friction coefficient values to increase.

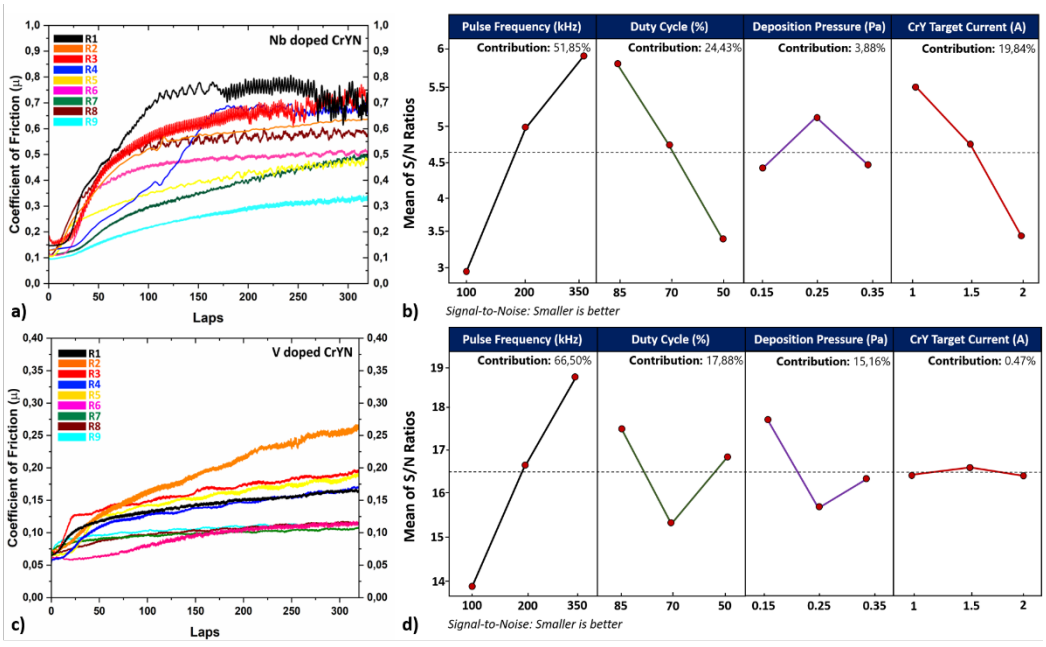

Fig 12. a) CoF value of Nb-doped thin films, **b)** average S/N Ratios for Nb-doped thin films in CoF, **c)** CoF value of V-doped thin films and **d)** average S/N ratios for V-doped thin films in CoF

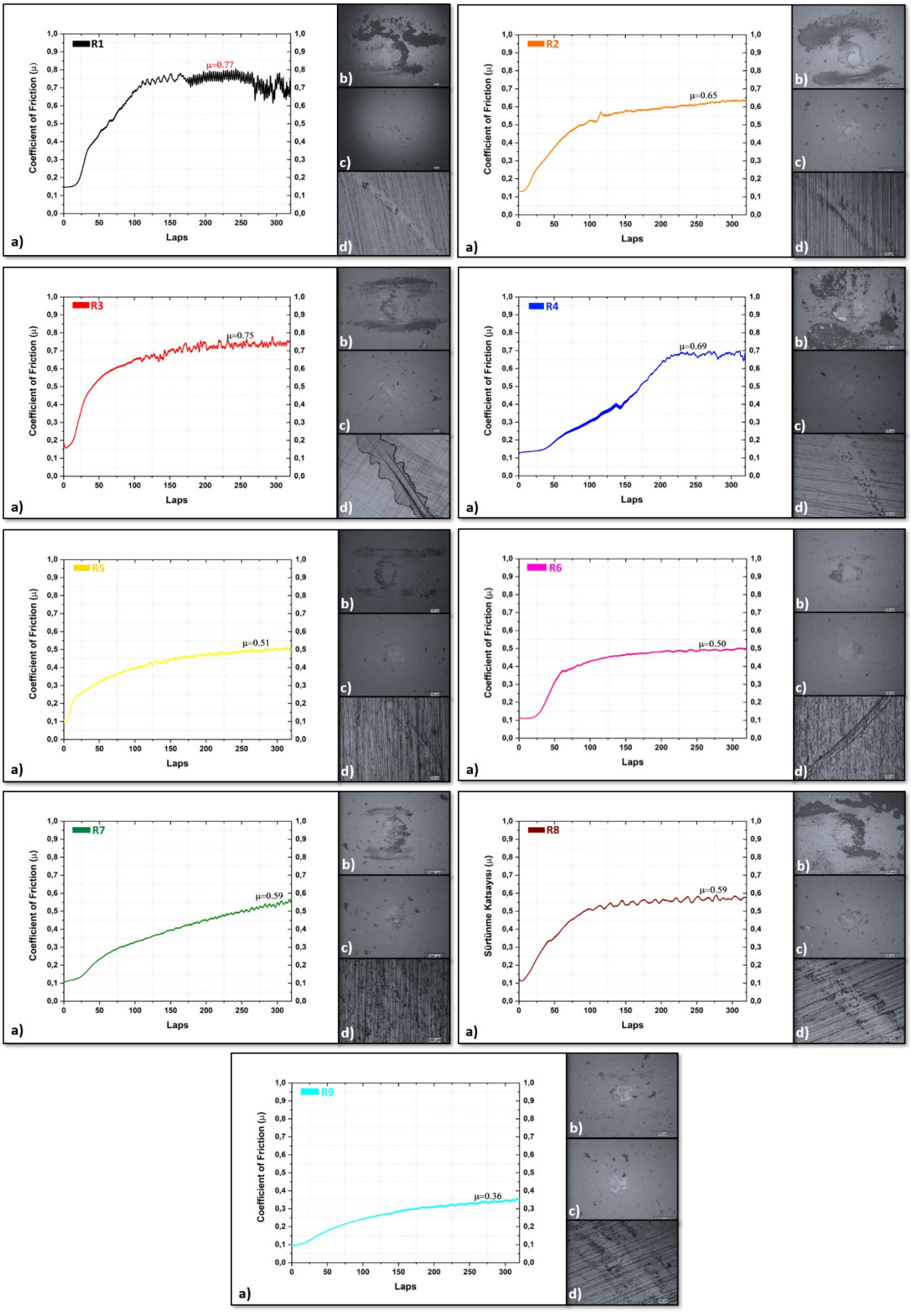

Fig 13. a) Coefficient of friction values, **b)** uncleaned Al_2O_3 pin surface **c)** cleaned Al_2O_3 pin surface, and **d)** wear scar images of Nb-doped CrYN thin films

When the friction tests (Fig. 12c) of the V-doped CrYN thin films performed under atmospheric conditions are examined, a linear behavior is observed. When the optical microscope images of the pin and wearing surfaces obtained after the friction test given in Fig. 14 are examined, it is clearly seen that very little wear debris is formed on the contact surfaces. This behavior supports a low coefficient of friction and a linear behavior. The S/N response showed in Figs. 11b and 11d was derived using the Taguchi DOE method in Minitab software, again ANOVA employed to evaluate the percentage contribution of various process parameters on the film coefficient of friction. As per Fig. 11b and 11d, the contribution levels of pulse frequency, duty cycle, deposition pressure, and CrY target current, as determined by the ANOVA analysis, are 51.85%, 24.43%, 3.88%, and 19.84% respectively for Nb-doped CrYN films. For V-doped CrYN thin films, the contribution levels of pulse frequency, duty cycle, deposition pressure, and CrY target current are 66.50%, 17.88%, 15.16%, and 0.47%, respectively. It can be seen that the most important parameter influencing CoF is pulse frequency.

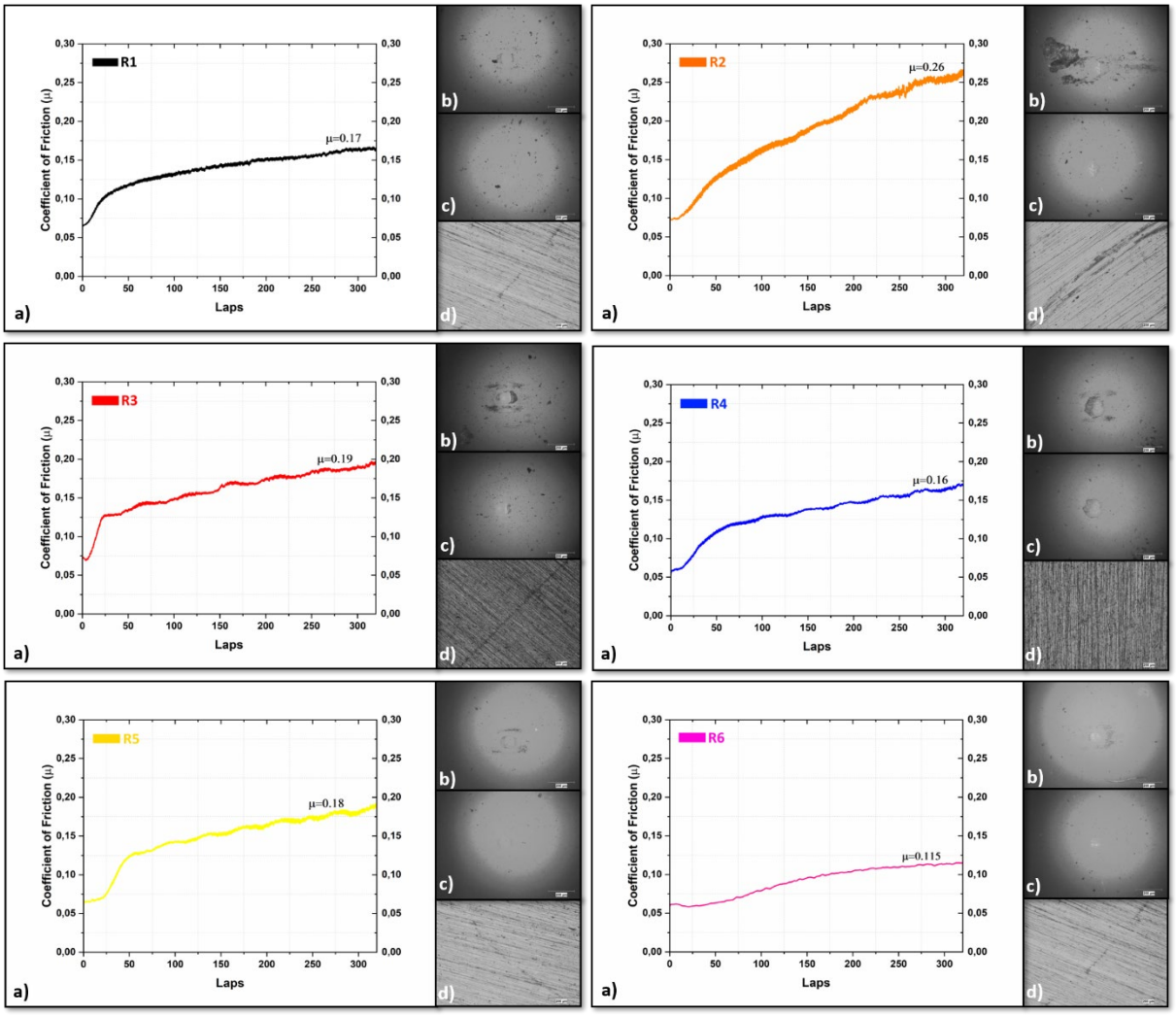

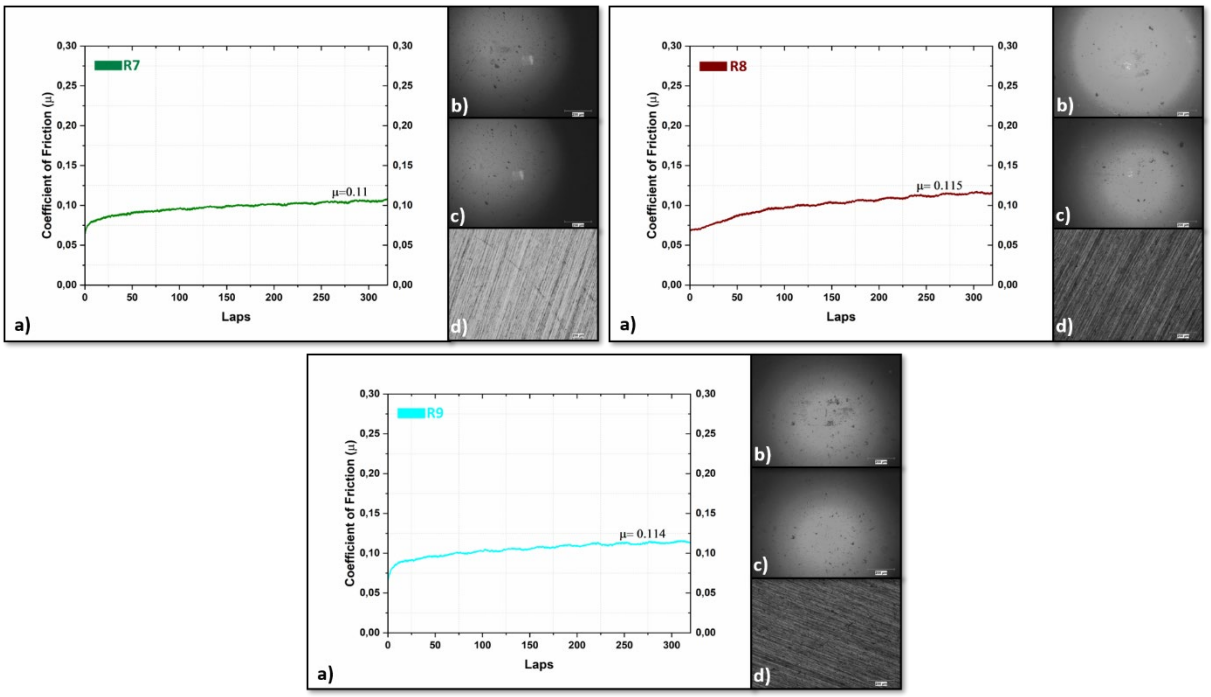

Fig 14. a) Coefficient of friction values, **b)** uncleaned Al_2O_3 pin surface **c)** cleaned Al_2O_3 pin surface, and **d)** wear scar images of V-doped CrYN thin films

4. Conclusions

Nb and V-doped CrYN thin films deposited by closed-field unbalanced magnetron sputtering (CFUBMS) under the different deposition parameters.

- Nb and V-doped CrYN thin films were successfully deposited on the 316L substrates, according to the XRD analysis. XRD peaks tend to shift towards a lower angle, due to compressive stress occurring in the coatings during sputtering. With an increase in pulse frequency, duty time and current applied to the CrY targets, the density of the CrN and Cr_2N crystal phases increases.
- Typical cross-sections of the Nb and V-doped CrYN thin films shown by SEM analysis showed the presence of a dense and uniform structure. After examining the film thicknesses from the cross-sectional micrographs, it can be noticed that the R3 for both doped films with the highest target current and lowest pulse frequency application had the thickest films.
- According to the microhardness values of the thin films, it was observed that the highest hardness value was 21.4 GPa in the Nb-doped thin films, while the highest hardness value was 16.1 GPa in the V-doped thin films. In addition, the highest hardness values in both types of films were obtained in the experiment where the pulse frequency was 100 kHz and the current applied to the CrY targets were 2A.

- Nb-doped and V-doped CrYN thin films were found to have excellent adhesion characteristics. Nb and V-doped CrYN thin films remained on the surface of the substrate in all tests up to 150N.
- The lowest friction coefficient was found to be 0.36 and the maximum friction coefficient was 0.77 in the Nb-doped thin films. The friction coefficients of V-doped thin films, in contrast, ranged from 0.1 to 0.26, which is quite low when compared to Nb-doped thin films. The wear particles at the contact point cause the higher friction coefficient of Nb-doped thin films compared to V-doped thin films.

Acknowledgements

This research was supported by Royal Society Projects (Grant Agreement No: IES\R2\202084) and Atatürk University-BAP (Grant Agreement No: FDA-2022-11399). The authors would like to thank to Royal Society and Atatürk University for funding the project.

References

[1] X. Li, W. Wu, H. Dong, Microstructural characterisation of carbon doped CrAlTiN nanoscale multilayer coatings, Surf Coat Technol. 205 (2011) 3251–3259. https://doi.org/10.1016/J.SURFCOAT.2010.11.046.

[2] Y.I. Chen, K.Y. Lin, C.C. Chou, Thermal stability of CrTaN hard coatings prepared using biased direct current sputter deposition, Thin Solid Films. 544 (2013) 606–611. https://doi.org/10.1016/J.TSF.2012.11.047.

[3] A. Keleş, H. Çiçek, Ö. Baran, Y. Totik, İ. Efeoğlu, Determining the critical loads of V and Nb doped ternary TiN-based coatings deposited using CFUBMS on steels, Surf Coat Technol. 332 (2017) 168–173. https://doi.org/10.1016/J.SURFCOAT.2017.07.085.

[4] Y. Ren, J. Jia, X. Cao, G. Zhang, Q. Ding, Effect of Ag contents on the microstructure and tribological behaviors of NbN–Ag coatings at elevated temperatures, Vacuum. 204 (2022) 111330. https://doi.org/10.1016/J.VACUUM.2022.111330.

[5] M.M. Al-Asadi, H.A. Al-Tameemi, A review of tribological properties and deposition methods for selected hard protective coatings, Tribol Int. 176 (2022) 107919. https://doi.org/10.1016/J.TRIBOINT.2022.107919.

[6] Y.C. Chim, X.Z. Ding, X.T. Zeng, S. Zhang, Oxidation resistance of TiN, CrN, TiAlN and CrAlN coatings deposited by lateral rotating cathode arc, Thin Solid Films. 517 (2009) 4845–4849. https://doi.org/10.1016/J.TSF.2009.03.038.

[7] D. Wang, M. Hu, D. Jiang, Y. Fu, Q. Wang, J. Yang, J. Sun, L. Weng, The improved corrosion resistance of sputtered CrN thin films with Cr-ion bombardment layer by layer, Vacuum. 143 (2017) 329–335. https://doi.org/10.1016/J.VACUUM.2017.06.040.

[8] Z. Li, Y. Wang, X. Cheng, Z. Zeng, J. Li, X. Lu, L. Wang, Q. Xue, Continuously Growing Ultrathick CrN Coating to Achieve High Load-Bearing Capacity and Good Tribological Property, ACS Appl Mater Interfaces. 10 (2018) 2965–2975. https://doi.org/10.1021/ACSAMI.7B16426/ASSET/IMAGES/AM-2017-164264_M007.GIF.

[9] J. Zhang, Z. Li, Y. Wang, S. Zhou, Y. Wang, Z. Zeng, J. Li, A new method to improve the tribological performance of metal nitride coating: A case study for CrN coating, Vacuum. 173 (2020) 109158. https://doi.org/10.1016/J.VACUUM.2019.109158.

[10] L. Kong, K. Huang, X. Cao, Z. Lu, G. Zhang, H. Hu, Effect of MoS2 content on friction and wear properties of Mo and S co-doped CrN coatings at 25–600 °C, Ceram Int. 47 (2021) 21450–21458. https://doi.org/10.1016/J.CERAMINT.2021.04.155.

[11] E. Mohammadpour, W.Y.H. Liew, N. Radevski, S. Lee, N. Mondinos, M. Altarawneh, M. Minakshi, A. Amri, M.R. Rowles, H.N. Lim, Z.T. Jiang, High temperature (up to 1200 °C) thermal-mechanical stability of Si and Ni doped CrN framework coatings, Journal of Materials Research and Technology. 14 (2021) 2406–2419. https://doi.org/10.1016/J.JMRT.2021.07.130.

[12] K. Huang, X. Cao, L. Kong, Z. Lu, G. Zhang, Q. Ding, H. Hu, Effect of Ag content on friction and wear properties of Ag and V co-doped CrN coatings at 25–700 °C, Ceram Int. 47 (2021) 35021–35028. https://doi.org/10.1016/J.CERAMINT.2021.09.043.

[13] D. Wang, S. sheng Lin, J. de Lu, S. qi Huang, Z. fu Yin, H. zhi Yang, P. ying Bian, Y. liang Zhang, M. jiang Dai, K. song Zhou, Research on high temperature wear resistance mechanism of CrN/CrAlN multilayer coatings, Tribol Int. 180 (2023) 108184. https://doi.org/10.1016/J.TRIBOINT.2022.108184.

[14] T.C. Rojas, S. El Mrabet, S. Domínguez-Meister, M. Brizuela, A. García-Luis, J.C. Sánchez-López, Chemical and microstructural characterization of (Y or Zr)-doped CrAlN coatings, Surf Coat Technol. 211 (2012) 104–110. https://doi.org/10.1016/J.SURFCOAT.2011.07.071.

[15] P. Hones, R. Sanjinés, F. Lévy, Sputter deposited chromium nitride based ternary compounds for hard coatings, Thin Solid Films. 332 (1998) 240–246. https://doi.org/10.1016/S0040-6090(98)00992-4.

[16] Y.Y. Chang, D.Y. Wang, Corrosion behavior of CrN coatings enhanced by niobium ion implantation, Surf Coat Technol. 188–189 (2004) 478–483. https://doi.org/10.1016/J.SURFCOAT.2004.08.057.

[17] B. Liu, B. Deng, Y. Tao, Influence of niobium ion implantation on the microstructure, mechanical and tribological properties of TiAlN/CrN nano-multilayer coatings, Surf Coat Technol. 240 (2014) 405–412. https://doi.org/10.1016/J.SURFCOAT.2013.12.065.

[18] M. Uchida, N. Nihira, A. Mitsuo, K. Toyoda, K. Kubota, T. Aizawa, Friction and wear properties of CrAlN and CrVN films deposited by cathodic arc ion plating method, Surf Coat Technol. 177–178 (2004) 627–630. https://doi.org/10.1016/S0257-8972(03)00937-X.

[19] L. Aissani, C. Nouveau, M.J. Walock, H. Djebaili, A. Djelloul, Influence of vanadium on structure, mechanical and tribological properties of CrN coatings, Http://Dx.Doi.Org/10.1179/1743294415Y.0000000043. 31 (2015) 779–788. https://doi.org/10.1179/1743294415Y.0000000043.

[20] I. Efeoglu, G. Gülten, B. Yaylalı, Y. Totik, P. Kelly, J. Kulczyk-Malecka, Development of coatings for hostile environments, 2022.

[21] N. Nedfors, A. Mockute, J. Palisaitis, P.O.Å. Persson, L.Å. Näslund, J. Rosen, Influence of pulse frequency and bias on microstructure and mechanical properties of TiB2 coatings deposited by high power impulse magnetron sputtering, Surf Coat Technol. 304 (2016) 203–210. https://doi.org/10.1016/J.SURFCOAT.2016.06.086.

[22] N. Nedfors, A. Mockute, J. Palisaitis, P.O.Å. Persson, L.Å. Näslund, J. Rosen, Influence of pulse frequency and bias on microstructure and mechanical properties of TiB2 coatings deposited by high power impulse magnetron sputtering, Surf Coat Technol. 304 (2016) 203–210. https://doi.org/10.1016/J.SURFCOAT.2016.06.086.

[23] P.J. Kelly, A.A. Onifade, Y. Zhou, G.C.B. Clarke, M. Audronis, J.W. Bradley, The Influence of Pulse Frequency and Duty on the Deposition Rate in Pulsed Magnetron Sputtering, Plasma Processes and Polymers. 4 (2007) 246–252. https://doi.org/10.1002/PPAP.200600159.

[24] C.-L. Chang, S.-G. Shih, P.-H. Chen, W.-C. Chen, C.-T. Ho, W.-Y. Wu, Effect of duty cycles on the deposition and characteristics of high power impulse magnetron sputtering deposited TiN thin films, (2014). https://doi.org/10.1016/j.surfcoat.2014.03.011.

[25] I. Bertóti, M. Mohai, P.H. Mayrhofer, C. Mitterer, Surface chemical changes induced by low-energy ion bombardment in chromium nitride layers, Surface and Interface Analysis. 34 (2002) 740–743. https://doi.org/10.1002/SIA.1401.

[26] M. Chen, S. Wang, J. Zhang, D. He, Y. Zhao, Synthesis of Stoichiometric and Bulk CrN through a Solid-State Ion-Exchange Reaction, Chemistry – A European Journal. 18 (2012) 15459–15463. https://doi.org/10.1002/CHEM.201202197.

[27] Z. Hui, X. Zuo, L. Ye, X. Wang, X. Zhu, Solution Processable CrN Thin Films: Thickness-Dependent Electrical Transport Properties, Materials 2020, Vol. 13, Page 417. 13 (2020) 417. https://doi.org/10.3390/MA13020417.

[28] I. Bertoti, Characterization of nitride coatings by XPS, Surf Coat Technol. (2002) 194–203. www.chemres.huyAKKL (accessed October 5, 2023).

[29] Z.T. Wu, Z.B. Qi, F.P. Zhu, B. Liu, Z.C. Wang, Influences of Y addition on mechanical properties and oxidation resistance of CrN coating, Phys Procedia. 50 (2013) 150–155. https://doi.org/10.1016/J.PHPRO.2013.11.025.

[30] P.J. Burnett, D.S. Rickerby, The scratch adhesion test: An elastic-plastic indentation analysis, Thin Solid Films. 157 (1988) 233–254. https://doi.org/10.1016/0040-6090(88)90006-5.